Imane Khalil
Shiley-Marcos Department of Mechanical Engineering, University of San Diego, 5998 Alcala Park, San Diego, CA 92110

Quinn Pratt
Shiley-Marcos Department of Mechanical Engineering, University of San Diego, 5998 Alcala Park, San Diego, CA 92110

Harrison Schmachtenberger
Shiley-Marcos Department of Mechanical Engineering, University of San Diego, 5998 Alcala Park, San Diego, CA 92110

Roger Ghanem
Sonny Astani Department of Civil and Environmental Engineering, 3610 S. Vermont Street, University of Southern California, Los Angeles, CA 90089

Heat Transfer Modeling of Spent Nuclear Fuel Using Uncertainty Quantification and Polynomial Chaos Expansion

A novel method that incorporates uncertainty quantification (UQ) into numerical simulations of heat transfer for a 9 × 9 square array of spent nuclear fuel (SNF) assemblies in a boiling water reactor (BWR) is presented in this paper. The results predict the maximum mean temperature at the center of the 9 × 9 BWR fuel assembly to be 462 K using a range of fuel burn-up power. Current related modeling techniques used to predict the heat transfer and the maximum temperature inside SNF assemblies rely on commercial codes and address the uncertainty in the input parameters by running separate simulations for different input parameters. The utility of leveraging polynomial chaos expansion (PCE) to develop a surrogate model that permits the efficient evaluation of the distribution of temperature and heat transfer while accounting for all uncertain input parameters to the model is explored and validated for a complex case of heat transfer that could be substituted with other problems of intricacy. UQ computational methods generated results that are encompassing continuous ranges of variable parameters that also served to conduct sensitivity analysis on heat transfer simulations of SNF assemblies with respect to physically relevant parameters. A two-dimensional (2D) model is used to describe the physical processes within the fuel assembly, and a second-order PCE is used to characterize the dependence of center temperature on ten input parameters. [DOI: 10.1115/1.4037501]

1 Introduction

In a nuclear reactor, an array of fuel rods made from zircaloy cladding tube containing stacked uranium dioxide (UO_2) pellets is the heat source for a thermodynamic cycle of energy conversion from heat to electricity.

Spent nuclear fuel (SNF) assemblies are composed of a square array of fuel rods supported by several grid spacers located along the length of the assemblies. Each fuel assembly is enclosed in a zircaloy sheath or channel box. Typical boiling water reactor (BWR) assemblies are composed of a square array of fuel rods that can vary from 7×7 to 9×9 grid while a typical pressure water reactor will vary between arrangements with 11×11, 13×13, and 15×15 grids [1].

After fuel is used in a nuclear reactor, the fuel pellets continue to generate heat. The spent fuel assemblies are stored underwater in a spent nuclear fuel pool at the nuclear power plant while heat generation and radioactive decay rates decrease [2,3]. The spent fuel is then placed in packages for dry storage or transportation. In these packages, individual fuel assemblies are supported within square cross section basket openings inside the cask containment volume. The cask containment unit is designed to contain radioactive materials, reduce decay heat, and shield against gamma and neutron radiation emitted by the fuel [4]. The containment region of the package is typically evacuated and then back-filled with a nonoxidizing, high thermal conductivity gas, typically helium [5]. The helium is slightly pressurized to induce a higher convective heat transfer rate. It has been demonstrated that higher gas density, or pressure, increases the convective heat transfer rate [6].

The amount of heat generated by UO_2 depends on the reactor burn-up and the postreactor pool cooling time. The heat is transferred through conduction within the fuel rods, convection and radiation across the gas-filled region between the rods, the enclosure, and the effective thermal resistance at the gas/solid interface. The fuel cladding must be maintained below the temperature limit of 400 °C as specified by the NRC Guidance, for normal conditions of storage, to avoid dissolution of circumferential hydrides inside the cladding and high gas pressures in the fuel containing sheaths, which leads to high hoop stress and reduce the integrity of the cladding [7].

Package designers must accurately predict a credible range for the temperature of the cladding that surrounds the pellets to ensure that it does not exceed its integrity temperature of 400 °C during normal transport [7].

The objective of the present study is to predict the maximum cladding temperatures using heat transfer simulations, using the commercial software FLUENT, of a BWR SNF assembly. The corresponding model considers a typical square array of fuel rods, enclosed and centered in a square basket in the horizontal position.

Researchers in this field used different computer codes in their studies and have presented numerical results for models of SNF assemblies. Still missing from the published literature, however, is a benchmark of regional material property models for the full range of applicable conditions, thus accurately reflecting uncertainty in the observed temperature. Previous studies have verified the general validity of numerical investigations concerning heat transfer in spent-fuel assemblies [8,9].

Current modeling techniques to predict the heat transfer and the maximum temperature inside spent nuclear fuel assemblies use FLUENT or similar analysis codes. They address the uncertainty in the input parameters by running separate simulations for a statistically representative selection of input parameters. As the number of these parameters increases, the number of required samples grows exponentially, resulting in prohibitively large computational burden. This has limited the extent of uncertainty quantification (UQ) used with these problems, resulting in questionable risk assessment. Polynomial chaos expansion (PCE) UQ is incorporated into the computer models in order to provide an efficient surrogate from which statistical samples can be drawn at will, resulting in confident predictions of ranges and tail distributions

Contributed by the Heat Transfer Division of ASME for publication in the JOURNAL OF HEAT TRANSFER. Manuscript received March 27, 2017; final manuscript received June 7, 2017; published online September 6, 2017. Editor: Portonovo S. Ayyaswamy.

of temperatures and heat transfer. This in turn has consequences on the credibility of associated risk assessment analysis. The approach and methodology developed for the case of spent nuclear fuel is modular in nature and could be harnessed to analyze sensitivity of variables to input parameters in other cases of engineering requiring elementwise operations.

Applying UQ methods to computational fluid dynamics (CFD) has been explored in the past [10]. Many studies incorporate variations using multiple individual simulations that fix all but one parameter that is then investigated through a series of tests [11]. These approaches ignore the effect of cross-coupling between the parameters, which could be significant for problems with complex underlying physics, such as the present case.

The PCE approach that characterizes the solution of stochastic differential equations is a transformative way of applying uncertainty analysis to model heat transfer for spent fuel assemblies and theoretically similarly complex systems.

2 Computational Model

The simulations performed for this study used the commercial FLUENT, version 17.0, by ANSYS. Figure 1 shows the cross section of the two-dimensional (2D) model representing a 9×9 fuel rod array stored horizontally with the rods parallel to the ground. The rods are made up of a UO_2 core surrounded by a zircaloy tube sheath. The void between the rods is filled with helium cover gas. The cover gas is contained within a zircaloy channel wall. There is helium in the space between the channel wall and the outermost enclosure. The enclosure is made of stainless steel. A detailed lower right corner of the geometry is shown in Fig. 2.

There are eighty-one fuel rods each of cladding outer diameter of 10.77 mm, UO_2 pellet diameter of 9.06 mm, and a cladding thickness of 0.76 mm [12,13]. Heat is assumed to be generated within the UO_2 cores uniformly. The variable parameters, and their respective ranges, are shown in Table 1. The minimum and maximum values in the table represent $\pm 10\%$ of the nominal values for each variable. The exception to this is in the case of the prescribed boundary wall temperature; in this case, an uncertain range of ± 5 K is used. Independent uniform distributions are assumed to hold over each of these intervals.

The primary concern of the present study is to determine the effects of uncertainty in various material properties and their influence on the temperature distribution inside the assembly. The

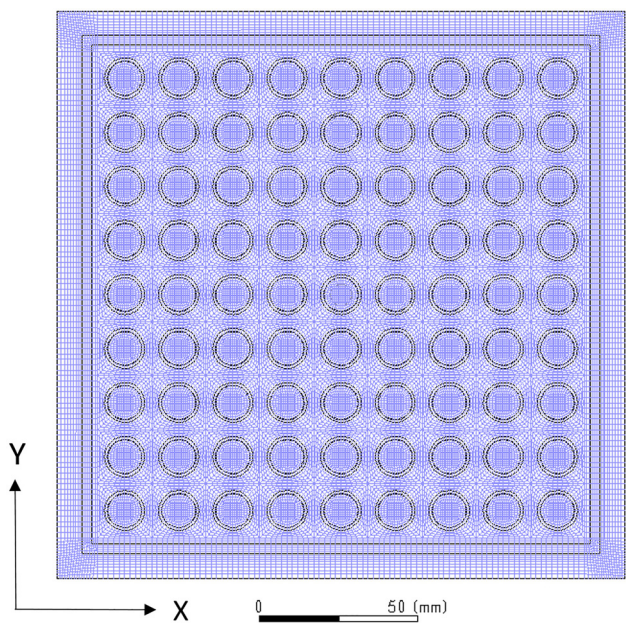

Fig. 1 FLUENT computational mesh for the 9 × 9 storage basket

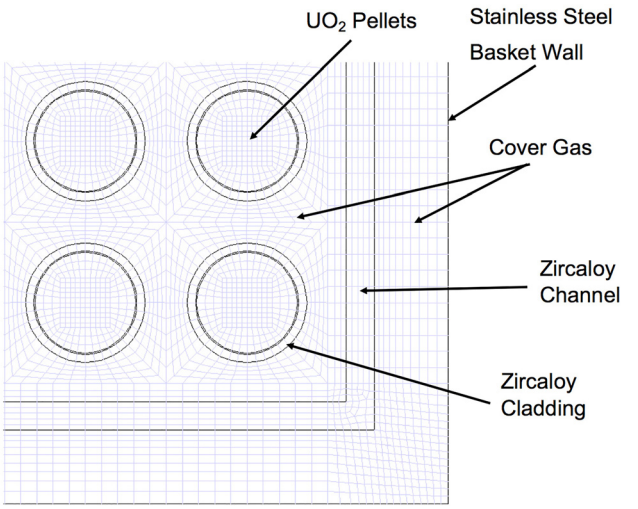

Fig. 2 Lower right corner of computational model of the 9 × 9 storage basket

Table 1 The ranges for the uncertainties in each of the ten input variables to the model

Variable parameters for $n = 10$, $p = 1$		
Variable	Minimum	Maximum
He, K (W/m · K)	0.1368	0.1672
He, C_p (J/kg · K)	4673	5712
Zr, K (W/m · K)	13.5	16.5
Zr, C_p (J/kg · K)	270	330
Zr, ε	0.8	1.0
UO_2, K (W/m · K)	4.5	5.5
UO_2, C_p (J/kg · K)	211.5	258.5
Wall temp (K)	415	425
Power [14] (W/m^3)	27,000	33,000
Fuel, ε	0.8	1.0

boundary wall temperature was prescribed at two distinct ranges. The first wall temperature range had a minimum value of 320 K and a maximum value of 325 K, and is referred to as the low wall temperature range. The second range has a minimum temperature of 420 K and a maximum value of 425 K, and is referred to as the high wall temperature range. These temperature values are typical for SNF assemblies in dry cask storage [15] and correspond, respectively, to storage assemblies placed near the outer boundary and near the center of the cask. Figure 3 shows a picture of a typical cask with multiple vertical assemblies inside it. Note that assemblies located in the center of the cask are expected to be hotter than assemblies located on the periphery.

A two-dimensional finite element computational model, with 79,953 elements, is used to describe the physics of the problem and to calculate the local temperature, pressure, and velocity. While a three-dimensional model would clearly provide a more accurate resolution of the physics, there is some evidence that a two-dimensional model, such as used in our present study, captures sufficiently well key features of the problem [16]. Further motivation for the present two-dimensional simulations is provided by the uncertainty quantification analysis. Indeed, with ten random material properties and a polynomial expansion of second-order, more than a thousand finite element simulations are conducted, a challenging task even with a two-dimensional model.

The heat transfer modes considered in the simulations are natural convection, conduction, and discrete ordinates radiation. Discrete ordinates radiation is the best suited radiation model for localized heat sources such as spent nuclear fuel rods [17]. The

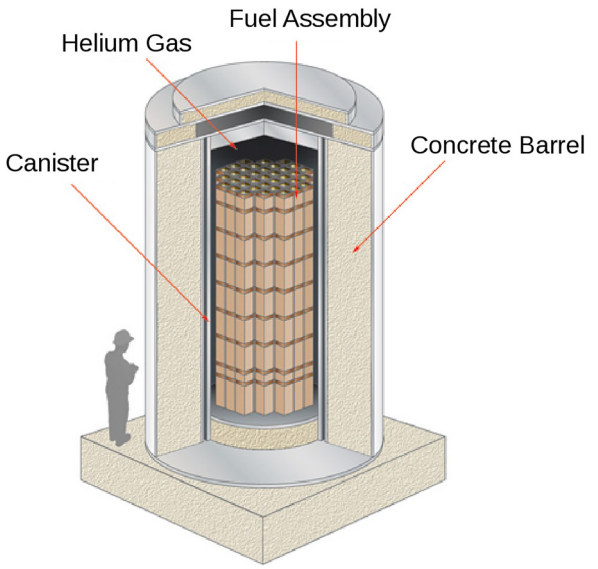

Fig. 3 Schematic of typical dry cask storage

outer wall of the assembly is held constant as per the Dirichlet assumption for heat transfer mechanics. In the scope of this study, gravitational effects were considered in the negative y-direction, which contributed to the convective heat transfer. The model is governed by the following equations:

The continuity equation is given as

$$\frac{\partial \rho}{\partial t} + \nabla \cdot (\rho U) = 0 \tag{1}$$

and the momentum equation as

$$\frac{\partial (\rho U)}{\partial t} + \nabla \cdot (\rho U \otimes U) = -\nabla p + \nabla \cdot \tau + S_M \tag{2}$$

where S_M is the momentum gained from external sources, and the stress tensor, τ, is related to the strain rate by

$$\tau = \mu \left(\nabla U + (\nabla U)^{\mathrm{T}} - \frac{2}{3} \delta \nabla \cdot U \right) \tag{3}$$

The total energy equation is given as

$$\frac{\partial (\rho h_{\mathrm{tot}})}{\partial t} - \frac{\partial p}{\partial t} + \nabla \cdot (\rho U h_{\mathrm{tot}}) = \nabla \cdot (\lambda \nabla \tau) + \nabla \cdot (UT) + U \cdot S_M + S_E \tag{4}$$

where h_{tot} is the total enthalpy, related to the static enthalpy $h(T, p)$ by

$$h_{\mathrm{tot}} = h + \frac{1}{2} U^2 \tag{5}$$

It should be noted that $\nabla \cdot (UT)$ represents the work due to viscous stresses and is negligible in most flows, and $U \cdot S_M$ represents the work due to external momentum sources and is also neglected [17].

3 Uncertainty Quantification

Uncertainty quantification, or UQ, is an emerging field for the scientific exploration at the interface between computational science, experimental science, and decision science. Specifically, it is relevant to the low risk requirements associated with nuclear fuel operations where complex phenomena necessitate reliance on detailed numerical resolution of physical processes. In this study, the PCE approach for characterizing and managing uncertainty was implemented [10,18]. This approach has been demonstrated on a wide range of applications relevant to present application, including computational fluid mechanics [10] and radioactive decay chemistry [19]. Due to the complexity of the geometry, and the variety of materials involved with SNF storage, there is a substantial amount of uncertainty inherent to many material properties. These material properties serve as inputs to a physical model. However, due to the range of uncertainty, and number of input properties, performing a standard parametric analysis is computationally prohibitive even on common high performance computing resources.

It is useful to begin with a review of PCE processes using a univariate example. Accordingly, a functional dependence of the quantities of interest, (Y), on an uncertain system parameter, (X), is expressed in the form

$$Y = F(X) \tag{6}$$

to better clarify the procedure we can consider the case where X is a scalar random variable, for instance X could be the thermal conductivity of the zircaloy in the model, and Y could be the maximum temperature in the basket. Assuming that the uncertainty in X to be due to microstructural variability, and associating that variability with a random variable ξ, both the input and output variables can be expressed by a polynomial expansion in terms of ξ yielding

$$\sum_{i=0}^{p} y_i \psi_i(\xi) = F(X(\xi)), \quad X(\xi) = \sum_{i=0}^{q} x_i \psi_i(\xi) \tag{7}$$

where ψ_i are polynomials orthogonal with respect to the probability measure of ξ. Thus, if ξ is assumed to be a Gaussian variable, ψ_i are taken as Hermite polynomials, while if ξ are assumed to be a uniform variable, ψ_i are Legendre polynomials in their arguments. The choice of distribution for ξ is a modeling decision that could reflect some physical or experimental evidence or expert opinion. In the present paper, ξ is considered to be a random variable with probability distribution over $[-1,1]$, and so the corresponding $\{\psi_i\}$ will be Legendre polynomials on the interval $[-1,1]$. Furthermore, the upper bound on the PCE expansion, p, is the highest order polynomial present in the output expansion. The coefficients x_i are evaluated such that the probability distribution of the parameter X is as close as possible to the distribution of $\sum_{i=0}^{q} x_i \psi_i(\xi)$. In the present analysis, however, this step is simplified as ξ is taken to be a linear normalized version of X (with zero mean and unit variance). Given the orthogonality of the Legendre polynomials, the coefficients y_i are given by

$$y_i = \frac{\langle F(X) \psi_i \rangle}{\langle \psi_i^2 \rangle} \tag{8}$$

where $\langle . \rangle$ denotes mathematical expectation with respect to the distribution of ξ. The denominator in this last equation is a constant that can be readily evaluated. The numerator, on the other hand, depends on the physics model and the associated numerical simulator and is evaluated as follows:

$$y_i = \langle F(X) \psi_i \rangle = \sum_{q=1}^{nq} F(X(\xi^{(q)})) \, \psi_i(\xi^{(q)}) w_q \tag{9}$$

where $\xi^{(q)}$ and w_q are quadrature abscissas and weights, respectively, used to evaluate the integral associated with the mathematical expectation. The choice of numerical quadrature is clearly important and should accommodate nonlinearities in both $F(X)$ and $\psi_i(\xi)$.

Once the coefficients y_i have been calculated, samples of Y can be synthesized very efficiently, thus allowing the accurate

construction of probability density functions (PDFs) and the evaluation of various relevant probabilities. Furthermore, the availability of an explicit functional dependence of Y on X permits the rapid assessment of key sensitivity coefficients. It is worth noting that y_0, the zeroth-order coefficient, is equal to the mean of Y, while its variance is given by $y_1^2 + \cdots + y_p^2$.

For the multidimensional case, where X is a vector of parameters, the above procedure is generalized by considering multidimensional polynomials in a vector-valued function of standard random variables ξ_i. Considering the case where X is vector consisting of n independent random variables, each component of X is mapped into a random variable ξ_i resulting in a random vector $\boldsymbol{\xi}$ of dimension n. A polynomial of order p in n dimensions will have N_{pc} terms where

$$N_{pc} = \frac{(n+p)!}{n!p!} \tag{10}$$

The multivariate polynomials $\Psi_i(\boldsymbol{\xi})$ are obtained as product of one-dimensional polynomials $\psi(\xi_i)$. Analogous to the univariate case, the general model expression, $Y = F(X)$, can be expanded in multivariate polynomial expansion of the form

$$\sum_{i=1}^{N_{pc}} y_i \Psi_i(\boldsymbol{\xi}) = F(X(\boldsymbol{\xi})), \quad y_i = \frac{\langle F(X)\Psi_i \rangle}{\langle \Psi_i^2 \rangle} \tag{11}$$

where now $\langle . \rangle$ refers to expectation with respect to the probability density function of the multivariate random vector $\boldsymbol{\xi}$. All of the UQ mathematics are handled through the MATLAB release of the Sandia National Labs UQToolkit [20–22]. Although ANSYS FLUENT was used for the modeling of the storage container, MATLAB was used for the UQ methodology applied to the CFD results of ANSYS. An iterative procedure was developed to create and combine case files and solution files from ANSYS and complete the analysis in the MATLAB environment.

The uncertainty of each parameter is treated as input to the MATLAB program. The UQToolkit creates a multivariate quadrature of multiple parameters, and each set of parameters represents a different CFD simulation. These parameters are mapped together and then directed into a FLUENT journal file, which is updated at each simulation. FLUENT will run thousands of simulations, each time producing solution data such as total temperature, velocity, and pressure. These solution files are then automatically imported into MATLAB and used in UQ analyses to evaluate the quadrature sums in Eq. (9).

4 First-Order Analysis

The first analysis was performed to assess the contributions to temperature distributions from the variable parameters in Table 1. With ten variable parameters (stochastic dimensions), a first-order Legendre polynomial was used in the uncertainty quantification calculations. To generate the data needed for the sensitivity analysis, 1024 FLUENT simulations were performed. The wall time on the local high performance computing cluster with 2 Intel Xeon E5 - 2.40 GHz (16 cores) processors was approximately 8 h.

Figure 4 shows the mean temperature profile (in Kelvin) for the simulation of dimension ten ($n = 10$) and Legendre polynomial order of one ($p = 1$) for the high boundary wall temperature. The difference between the maximum temperature (at the center) and the minimum temperature (at the wall) is roughly 30 K. The hottest point is at the center of the assembly, as expected, and reaches 449 K.

Figure 5 shows the mean temperature profile for the low boundary wall temperature case. In this case, the difference between the maximum temperature (at the center) and the minimum temperature (at the wall) is roughly 40 K, making this a higher temperature gradient than the high wall temperature case. The hottest point at the center of the assembly reaches 358 K.

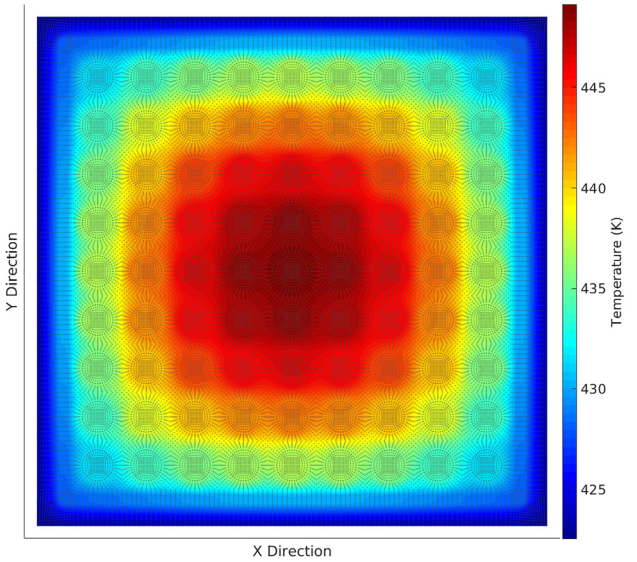

Fig. 4 Mean temperature (Kelvin) throughout the assembly for high boundary wall temperature

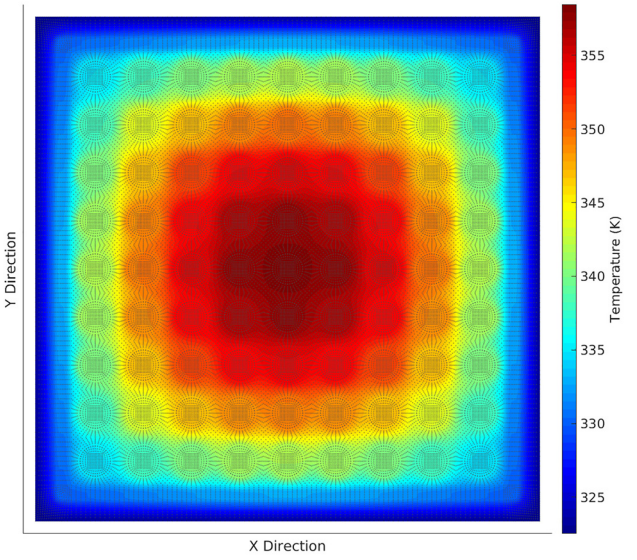

Fig. 5 Mean temperature (Kelvin) throughout the assembly for low boundary wall temperature

Figures 6 and 7 show the probability density function PDF of the temperature at the center of the 9×9 assembly for the high and low boundary wall temperatures, respectively.

The buffer gas velocity in the assembly for the high boundary wall temperature case is shown in Fig. 8. In an enclosed volume subject to gravity, as in this case, heated fluids naturally circulate according to archetypal natural convection cells. As expected, these cells are shown by the streamlines in Fig. 8. In the center, the hot gases rise to the top of the assembly and then move to the outer walls where they are cooled and flow down by gravity. This circulation has been observed in studies with similar geometries and parameters as well [3].

For the high boundary wall temperature case, there is a maximum y-component of velocity equal to 0.3 cm/s, whereas in the low boundary wall temperature case, the maximum y-component of velocity is 0.5 cm/s. Similarly, in the high boundary wall temperature case, there is a maximum velocity *magnitude* of 0.23 cm/s, and in the low boundary wall temperature case, there is a maximum

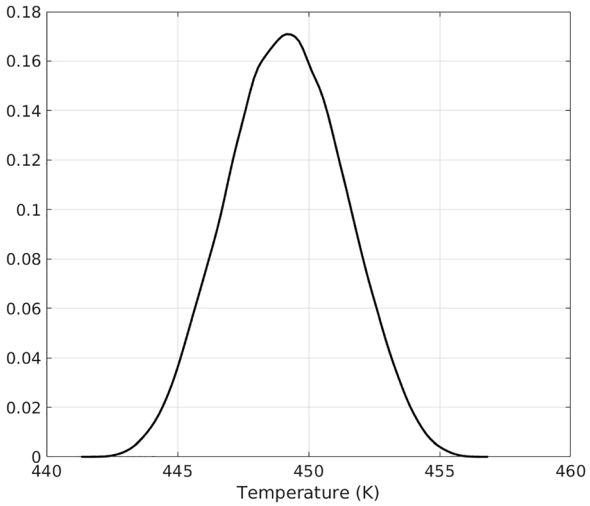

Fig. 6 PDF for the center temperature in the high boundary wall temperature case

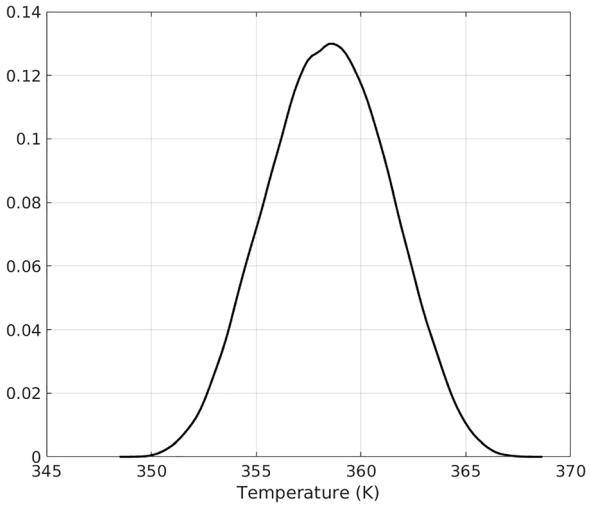

Fig. 7 PDF for the center temperature in the low boundary wall temperature case

velocity magnitude of 0.69 cm/s. This is due to the higher motivating gradient for heat transfer in the case with the lower prescribed boundary wall temperature. A similar study found velocities between 0.01 and 1.0 cm/s using air as the buffer gas instead of helium [23]. Another study, using helium with wall boundary temperatures of 25 °C and 400 °C, found velocities between 0.01 and 1.0 cm/s as well in an 8×8 array [24].

The coefficient of variation (COV), σ/μ, for temperature was calculated at each point in the mesh to determine areas sensitive to variation in input model parameters. Figure 9 shows a surface of the COV, which indicates that the center of the fuel assembly has the highest coefficient of variation, and thus the largest sensitivity to uncertainty.

The output expansion for the center temperature is a polynomial with ten terms. The terms and their associated coefficients are given in Table 2. The second column contains the coefficients from the low boundary wall temperature case with a range of 320–325 K, while column three contains the coefficients from the high boundary wall temperature case with a range of 420–425 K as described above.

The coefficients represent the sensitivity to uncertainty for the output temperature at the center of the assembly. It is clear from Table 2 that uncertainty in the boundary wall temperature (Wall T) and uncertainty in the power released by the uranium dioxide (power) have the largest effect on the maximum temperature. Similar studies have shown that heat generation rate (power) is the most influential factor in peak temperatures [25].

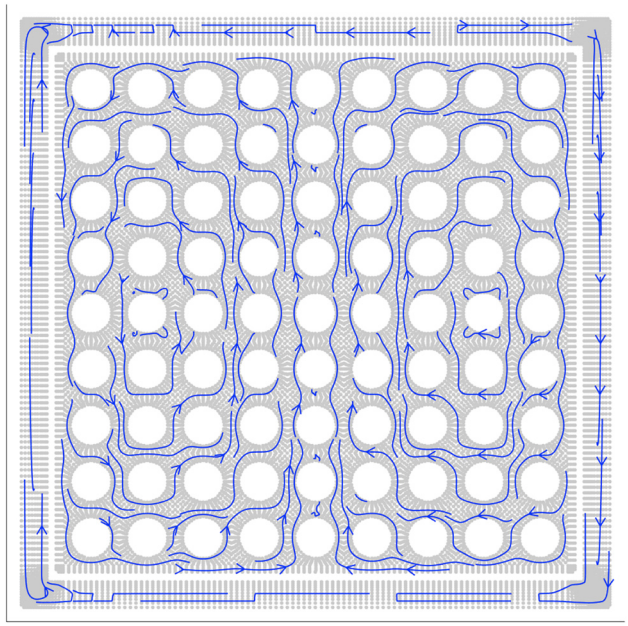

Fig. 8 Mean velocity streamlines for high boundary wall temperature case

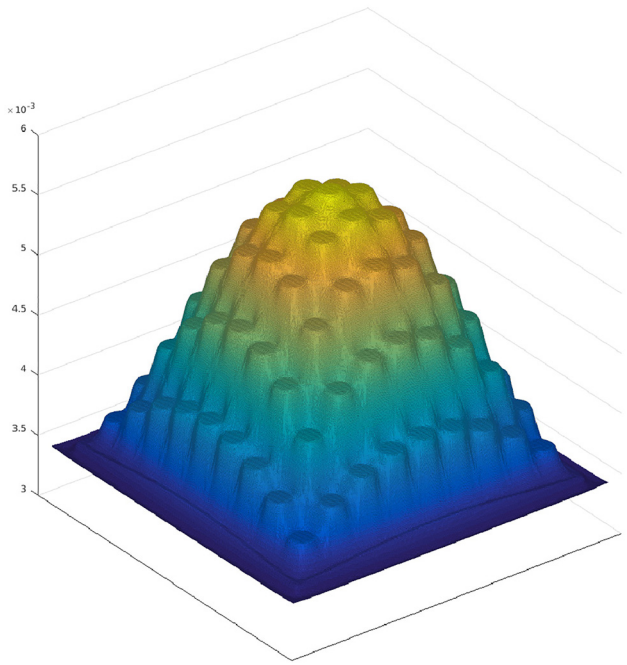

Fig. 9 Perspective view of the COV at each point in the mesh; predictions about the center of the basket will typically exhibit more variation

The temperature's sensitivity to the uncertainty in the specific heat of helium (He C_p) is relatively unchanged whether the boundary wall temperature is high or low. Evidently, uncertainty in the specific heat of helium has little influence on the maximum temperature.

The sensitivity to the uncertainty in specific heat of zircaloy (Zr C_p) and the specific heat of the UO_2 (UO_2 C_p) increase by many orders of magnitude in the higher boundary wall temperature case.

Table 2 Coefficients from the $n = 10$, $p = 1$ simulations at low and high boundary wall temperature

Term	Low WallT	High WallT
He K	−2.366	−1.111
He C_p	-0.856×10^{-3}	-0.1258×10^{-3}
Zr K	–0.0980	0.02936
Zr C_p	-8.881×10^{-15}	0.1012
Zr ε	−1.303	−1.486
UO_2 K	−0.0483	−0.03772
UO_2 C_p	-2.665×10^{-14}	−0.1012
Wall T	3.480	2.5325
Power	3.480	2.535
Fuel ε	−0.0121	0.03489

This result was not expected as the specific heat for zircaloy and uranium dioxide (both solids) should continue to have small effects on convective heat transfer.

Separate FLUENT simulations were performed to calculate the maximum temperature at the center of the assembly while varying the specific heat for the solid materials over many orders of magnitude. The results showed minimal effect when changing Zr C_p and UO_2 C_p on the maximum temperature. This is expected because convection and radiation are the dominant modes of heat transfer. Therefore, the apparent increase in sensitivity to uncertainty in specific heat of the solid materials may be due to coupling effects. Coupling refers to the interaction of simultaneously varying multiple input parameters as is done in UQ analysis. Future work will further investigate the coupling effect in this model.

5 Sensitivity Analysis

The temperature's spatial sensitivity to uncertainty in each of the ten input parameters was analyzed through the UQ Sobol indices [21]. This allows us to examine specific locations in the assembly and their sensitivity to uncertainty in a particular input parameter.

For Figs. 10–15, it is evident that the temperature at the boundary is not sensitive to any of the properties; this is expected because the boundary wall temperature is prescribed and is therefore deterministic. However, at other points in the mesh, the final output temperature of the model is sensitive to variations in input parameters. Many of these figures show interesting spatial dependence on the temperature's sensitivity to uncertainty in a given material property, each indicating a physical process.

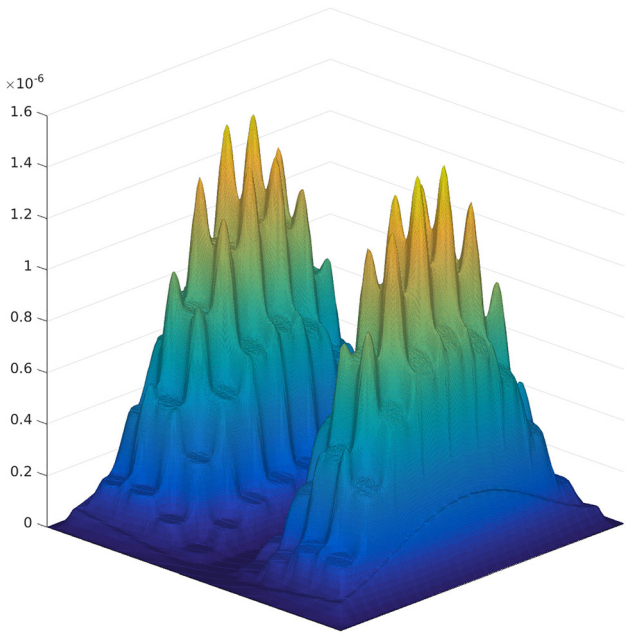

Fig. 10 Spatial dependence of the sensitivity of the temperature with respect to variations in the specific heat of helium

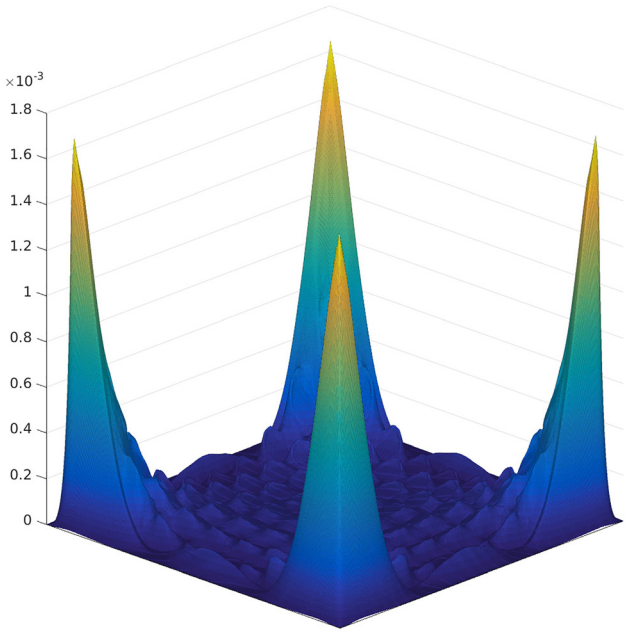

Fig. 11 Spatial dependence of the sensitivity of the temperature with respect to variations in the thermal conductivity of zircaloy for the high boundary wall temperature case

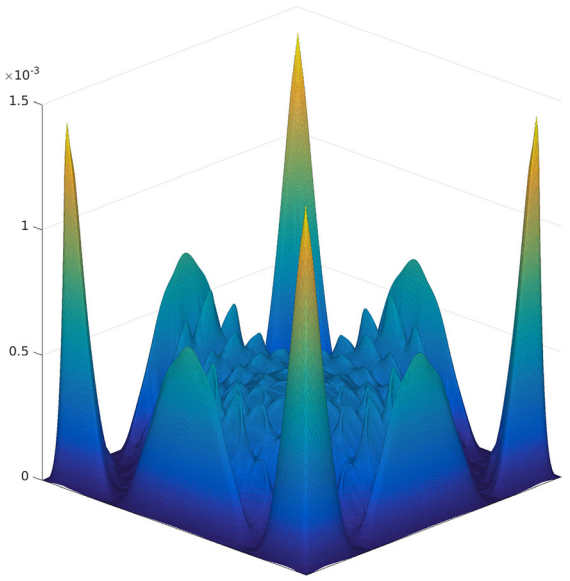

Fig. 12 Spatial dependence of the sensitivity of the temperature with respect to variations in the thermal conductivity of zircaloy for the low boundary wall temperature case

Figure 10 shows the temperature sensitivity to variation in the specific heat of helium (He C_p). The large spikes are indicative of the helium convection cells which facilitate natural convective heat transfer [3]. The spikes occur at the points between the fuel cores. The two clusters of spikes show that in the locations where the buffer gas is moving the least, it is the most sensitive to uncertainty in the specific heat. This is to be expected because specific heat indicates the amount of energy absorbed per change in temperature before transmitting said energy kinetically (i.e., through

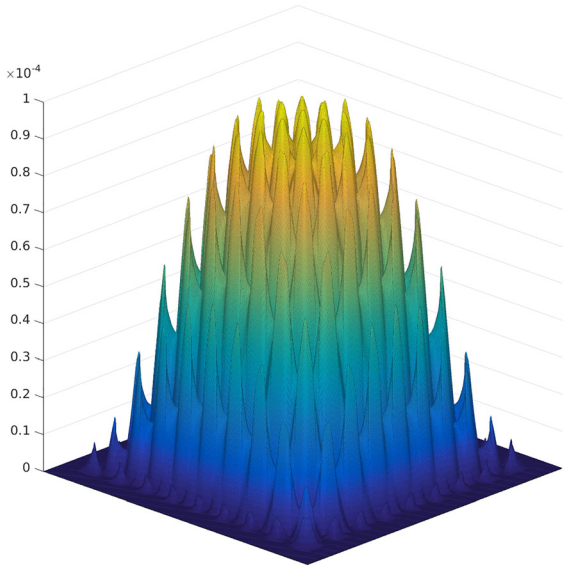

Fig. 13 Spatial dependence of the sensitivity of the temperature with respect to variations in the thermal conductivity of UO_2 for the high boundary wall temperature case

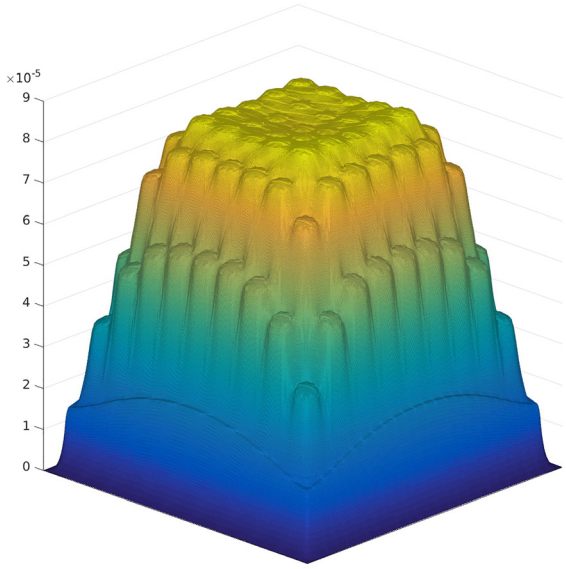

Fig. 14 Spatial dependence of the sensitivity of the temperature with respect to variations in the fuel emissivity for the high boundary wall temperature case

motion). Note that the clusters of spikes are in accordance with the two convection loops shown in Fig. 8.

In Figs. 11 and 12, the temperature sensitivity to uncertainty in the thermal conductivity of zircaloy is shown. Recall, each fuel rod is made of zircaloy containing the stacked fuel pellets. Additionally, the fuel assembly is enclosed in a zircaloy channel. The high boundary wall temperature case, shown in Fig. 11, indicates the location of the corners of the zircaloy channel to be the most sensitive to uncertainty in Zr K. However, at low boundary wall temperature, the zircaloy tubes, in the interior, become sensitive as per Fig. 12. This is due to the increase in the temperature difference between the wall temperature and the center temperature (ΔT), therefore making the conduction for zircaloy tube more important at low boundary wall temperature.

Figure 13 shows the sensitivity to uncertainty in the thermal conductivity of uranium dioxide. Uranium dioxide is the

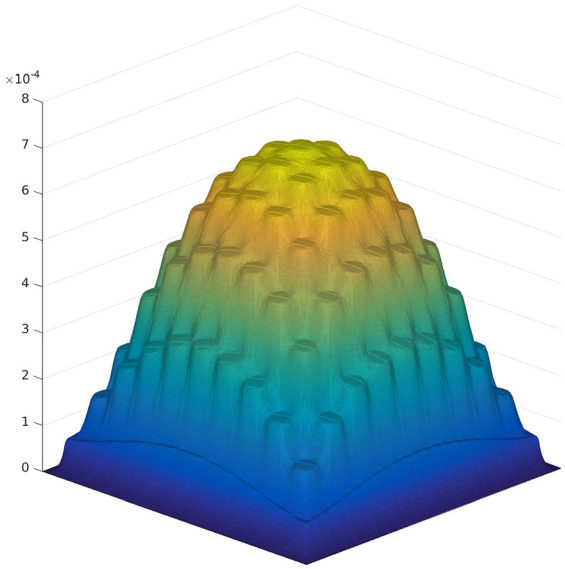

Fig. 15 Spatial dependence of the sensitivity of the temperature with respect to variations in the specific heat of the UO_2 for the high boundary wall temperature case

innermost component of the fuel rods. Inside each fuel rod, the variation of the sensitivity as a function of fuel rod location is shown as pointing inward toward the center of the assembly with the highest value at the edge of the fuel rods facing the outside wall of the assembly. This variation demonstrates the direction of heat transfer by conduction inside fuel rods from the center of the assembly to the outside wall. In addition, the hotter fuel rods at the center of the assembly display the largest sensitivity, which is an expected result as per Fig. 9.

Figure 14 shows the temperature's sensitivity to variation in the emissivity of the fuel rods. The flat top for the center fuel rods indicates a dominant radiation heat transfer mode at the center of the assembly but radiation mode drops abruptly near the boundary wall where the radiation effect is lower as the temperature goes down.

As many of the sensitivity surfaces share features nearly identical to Fig. 15, they were not included. The recurring "dome" shape is indicative that the most sensitive area is at the center, and the least sensitive area is at the boundary. This is expected due to the shape of the COV surface, Fig. 9.

6 Second-Order Analysis

In order to refine the model and test its dependency on second-order terms in the polynomial expansion, four terms with negligible contribution were removed from the list of dimensions, casting them as deterministic. A second-order expansion was pursued in the remaining six parameters, resulting in the n6p2 representation.

Figure 16 shows the comparison in the PDFs for the first-order polynomial expansion with respect to the second-order polynomial expansion. Both cases featured a high wall temperature with fluctuations between 420 K and 425 K, and nominal power from the fuel rods (as per Table 1).

Table 3 shows several parameters displayed low coefficients of significance; the terms including specific heat for zircaloy and UO_2 as well as Fuel emissivity and conductivity were removed from the variable parameters input for the subsequent convergence simulations with higher order polynomials. The second-order polynomial with six dimensions necessitated 729 FLUENT simulations.

7 Higher Heat Decay

The assembly heat generation rate value of 600 W used in this paper was taken from a study by Oak Ridge National Laboratory

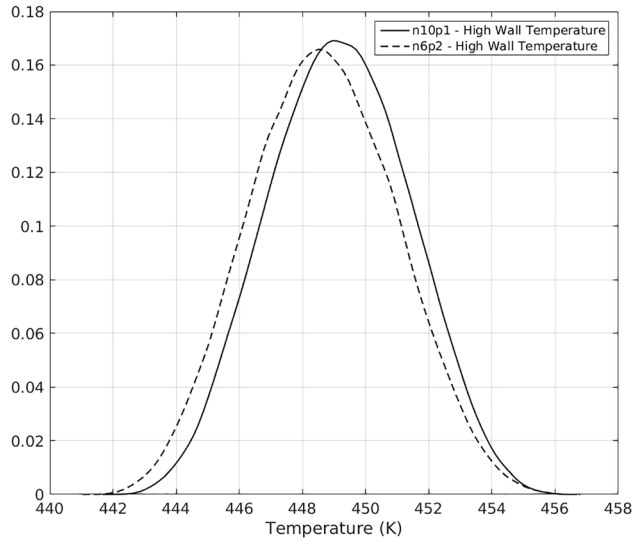

Fig. 16 Comparison of the PDFs for the center temperature created from the $n = 6$, $p = 2$ and $n = 10$, $p = 1$ simulations

Table 3 Effect of dropping several terms and increasing the order of the simulation from $p = 1$ to $p = 2$ for the high boundary wall temperature case

Term	n10p1	n6p2
He, K	−1.111	−1.2249
He, C_p	-0.1258×10^{-3}	—
Zr, K	0.02936	–0.0522
Zr, C_p	0.1012	0
Zr, ε	−1.486	−1.5644
UO_2, K	−0.03772	—
UO_2, C_p	−0.1012	—
Wall T	2.5325	2.269
Power	2.535	2.590
Fuel, ε	0.03489	—

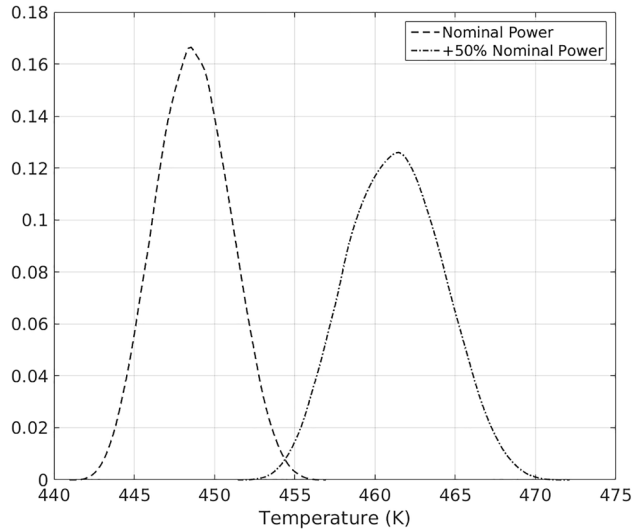

Fig. 17 Comparison between the PDFs for the center temperature, the hotter one being the result of +50% heat generation rate

and was based on 5000 days in spent fuel pool after discharge from the reactor [14]. Removing the spent fuel from the pool before 5000 days can be beneficial and will clear up space for the new fresh fuel. The heat generation rate (power) was increased to 900 W (50% higher) for the following tests.

Figure 17 shows the PDF of the increased heat generation rate and compares it to the original PDF of the nominal power for $n = 6$, $p = 2$ simulations. Both cases were performed assuming a high boundary wall temperature. Note that the maximum temperature limit is 673 K.

8 Conclusion and Future Work

A two-dimensional model representing a 9×9 spent fuel assembly stored horizontally is constructed using ANSYS FLUENT code. Polynomial chaos expansion was used to incorporate uncertainty quantification into the FLUENT model and address the uncertainty in the input parameters for helium, zircaloy, and UO_2. Steady-state simulations for heat transfer including the effect of natural convection and buoyancy induced gas motion, along with radiation and conduction through gas and solid regions were performed for different ranges of wall boundary temperature and different heat generation rates.

The implementation of the uncertainty quantification method and sensitivity analysis indicated that variation in the specific heats of the back fill gas, the zircaloy cladding, and the uranium pellets have no significant impact on the peak temperature at the center of the assembly. The analysis also indicated that variation in the boundary wall temperature and the heat generation released by UO_2 have the largest effect on the peak temperature inside the assembly.

For the case of an assembly with high boundary wall temperature varying between 420 K and 425 K, the peak mean temperature is at the center of the assembly, as expected, and reached a value of 449 K. Increasing the heat generation rate by 50% did increase the mean center temperature from 449 K to 462 K, which is still below the maximum temperature limit of 400 °C (673 K). Exploring the effect of higher heat generation rates will be recommended for future studies. Calculating the maximum allowable heat generation that brings the peak temperature in the assembly to the radial hydride formation limit ($T = 400$ °C) will allow storing the fuel for a shorter time in the spent fuel pool, therefore allowing space for the new fuel coming out of the reactors.

A three-dimensional FLUENT model will be created for future simulations. Previous studies have shown that two-dimensional simulations overestimate the temperature in SNF assembly holding canisters [15]. The uncertainty quantification method could be used to reduce the computational intensity required by large assemblies due to a large number of nodes. This computational cost is typically mitigated by the use of an effective thermal conductivity. The same input variables will be examined as well as grouped material properties wherein individual parameters such as helium thermal conductivity and zircaloy thermal conductivity will be controlled with one varied thermal conductivity. The same approach of uncertainty quantification combined with MATLAB data analysis will be accelerated with the utilization of a supercomputer cluster.

This developed methodology can be applied to other complex systems of heat transfer that are currently solved numerically. The technique has value beyond the scope of spent nuclear fuel simulations. The ability to determine the sensitivity of characteristics of interest with respect to many input parameters or combinations of input parameters is invaluable. The accuracy gained by creating a continuous distribution of those input parameters and determining the effective influence of that parameter in that range rather than discrete points is also of great importance with regard to the field of computational heat transfer.

Acknowledgment

The findings presented herein are those of the authors and do not necessarily reflect the views of the sponsor.

Funding Data

- Nuclear Energy University Program, U.S. Department of Energy (Award No. DE-NE0008529).

References

[1] DOE, 1987, "Characteristics of Spent Fuel, High-Level Waste, and Other Radioactive Wastes Which May Require Long-Term Isolation," Office of Civilian Radioactive Waste Management, Oak Ridge National Laboratory, Oak Ridge, TN, Technical Report No. DOE RW-0184.

[2] Saling, J. H., and Fentiman, W. A., 2002, *Radioactive Waste Management*, 2nd ed., Taylor and Francis, New York.

[3] Greiner, M., Araya, P., Chalasani, N. R., Li, J., and Liu, Y., 2013, "Two-Dimensional CFD Simulations of a Square 8x8 Heater Rod Array in an Isothermal Enclosure Filled With Rarified Air," International High-Level Radioactive Waste Management Conference (IHLRWMC), Albuquerque, NM, April 28–May 2, pp. 831–840.

[4] Greene, S., Medford, J. S., and Macy, S. A., 2013, "Storage and Transport Cask Data for Used Commercial Nuclear Fuel," Advanced Technology Insights LLC, Oak Ridge, TN, Technical Report No. ATI-TR-13047.

[5] Kessler, J., 2010, "Industry Spent Fuel Storage Handbook," Electric Power Research Institute, Palo Alto, CA, Technical Report No. 1021048.

[6] Saidi, M., and Hosseini Abardeh, R., 2010, "Air Pressure Dependence of Natural-Convection Heat Transfer," World Congress on Engineering (WCE), London, June 30–July 2, pp. 1444–1447.

[7] NRC, 2003, "Cladding Considerations for the Transportation and Storage of Spent Fuel," Spent Fuel Project Office Interim Staff Guidance-11, Revision 3, Nuclear Regulatory Commission, Washington, DC, Technical Report No. ISG-11 R3.

[8] Canaan, R. E., and Klein, D. E., 1998, "A Numerical Investigation of Natural Convection Heat Transfer Within Horizontal Spent-Fuel Assemblies," Nucl. Technol., **123**(2), pp. 193–208.

[9] Araya, P. E., and Greiner, M., 2009, "Benchmark of Natural Convection/Radiation Simulations Within an Enclosed Array of Horizontal Heated Rods," Nucl. Technol., **167**(3), pp. 384–394.

[10] Najm, H., 2009, "Uncertainty Quantification and Polynomial Chaos Techniques in Computational Fluid Dynamics," Annu. Rev. Fluid Mech., **41**(1), pp. 35–52.

[11] Cuta, J. M., Suffield, S. R., Fort, J. A., and Adkins, H. E., 2013, "Thermal Performance Sensitivity Studies in Support of Material Modeling for Extended Storage of Used Nuclear Fuel," TRW Environmental Safety Systems, Inc., Las Vegas, NV, Report No. PNNL-22646.

[12] Bahney, R., and Lotz, L. T., 1996, "Spent Nuclear Fuel Effective Thermal Conductivity Report," U.S. Department of Energy, Las Vegas, NV, Technical Report No. BBA000000-01717-5705-00010 Rev 00.

[13] Moore, R. S., and Notz, K. J., 1989, "Physical Characteristics of GE [General Electric] BWR [Boiling-Water Reactor] Fuel Assemblies," Oak Ridge National Laboratory, Oak Ridge, TN, Technical Report No. ORNL/TM-10902.

[14] Ade, B. J., and Gauld, I. C., 2011, "Decay Heat Calculations for PWR and BWR Assemblies Fueled With Uranium and Plutonium Mixed Oxide Fuel Using Scale," Oak Ridge National Laboratory, Oak Ridge, TN, Technical Report No. ORNL/TM-2011/290.

[15] Manzo, T., Nacer, M.-H., and Greiner, M., 2015, "Geometrically-Accurate-Three-Dimensional Simulations of a Used Nuclear Fuel Canister Filled With Helium," ASME Paper No. PVP2015-45851.

[16] Hyungjin, K., Kwon, O. H., Kang, G.-U., and Lee, D.-G., 2014, "Comparisons of Prediction Methods for Peak Cladding Temperature and Effective Thermal Conductivity in Spent Fuel Assemblies of Transportation/Storage Casks," Ann. Nucl. Energy, **71**, pp. 427–435.

[17] ANSYS, 2016, "ANSYS Commercial Release 16.2 User-Manual," ANSYS Inc., Canonsburg, PA.

[18] Ghanem, R., and Spanos, P., 1991, *Stochastic Finite Elements: A Spectral Approach*. Springer-Verlag, New York.

[19] Salloum, M., and Gharagozloo, P. E., 2014, "Empirical and Physics-Based Mathematical Models of Uranium Hydride Decomposition Kinetics With Quantified Uncertainty," Chem. Eng. Sci., **116**, pp. 452–464.

[20] Debusschere, B., Safta, C., Sargsyan, K., Chowdhary, K., Alexanderian, A., Salloum, M., Najm, H., Knio, O., Ghanem, R., and Adalsteinsson, H., 2015, *The Uncertainty Quantification Toolkit (UQTk)*, 1st ed., Sandia National Laboratory, Albuquerque, NM.

[21] Debusschere, B., Najm, H. N., Pebay, P. P., Knio, O. M., Ghanem, R. G., and Le Maitre, O. P., 2005, "Numerical Challenges in the Use of Polynomial Chaos Representations for Stochastic Processes," SIAM J. Sci. Comput., **26**(2), pp. 698–719.

[22] Ghanem, R., and Higdon, D. O. H., 2017, *Handbook of Uncertainty Quantification*, Vol. 1, Springer-Verlag, Cham, Switzerland.

[23] Araya, P. E., and Greiner, M., 2008, "CFD Simulations of an 8x8 Rod Array Inside of an Isothermal Enclosure Filled With a Rarefied Gas," ASME Paper No. PVP2008-61582.

[24] Greiner, M., and Araya, P., 2007, "Two-Dimensional Simulations of Natural Convection/Radiation Heat Transfer for BWR Assembly Within Isothermal Enclosure," Packag. Transp. Storage Secur. Radioact. Mater., **18**(3), pp. 171–179.

[25] Hadj-Nacer, M., Manzo, T., Ho, M., Graur, I., and Greiner, M., 2015, "Phenomena Affecting Used Nuclear Fuel Cladding Temperatures During Vacuum Drying Operations," International High-Level Radioactive Waste Management Conference (IHLRWM), Charleston, SC, Apr. 12–16, pp. 501–508.